Quantum wire with periodic serial structure

Hua Wu
Department of Physics and Astronomy, McMaster University, Hamilton, Ontario, Canada L8S 4M1

D.W.L. Sprung*
Institut für Kernphysik, Johannes Gutenberg-Universität, D-6500 Mainz, Germany

J. Martorell
Departamento d'Estructura de la Materia, Facultat Física, Universitat de Barcelona, E-08028 Barcelona, Spain

S. Klarsfeld
Division de Physique Théorique, IPN, F-91406 Orsay CEDEX, France
(Received 6 March 1991)

Electron wave motion in a quantum wire with periodic structure is treated by direct solution of the Schrödinger equation as a mode-matching problem. Our method is particularly useful for a wire consisting of several distinct units, where the total transfer matrix for wave propagation is just the product of those for its basic units. It is generally applicable to any linearly connected serial device, and it can be implemented on a small computer. The one-dimensional mesoscopic crystal recently considered by Ulloa, Castaño, and Kirczenow [Phys. Rev. B **41**, 12 350 (1990)] is discussed with our method, and is shown to be a strictly one-dimensional problem. Electron motion in the multiple-stub T-shaped potential well considered by Sols *et al.* [J. Appl. Phys. **66**, 3892 (1989)] is also treated. A structure combining features of both of these is investigated.

I. INTRODUCTION

Recently, considerable interest has been focused on mesoscopic systems within which the motion of electrons is governed by quantum mechanics rather than classical mechanics. In particular, the propagation of electrons along quantum wires of various geometries has been considered extensively.[1–3] More specifically, Sols *et al.*[4], Weisshaar *et al.*,[5] Avishai and Band,[6] and ourselves[7] have carried out calculations for a T-shaped device consisting of a main wire of constant width and a stub of similar width perpendicular to the wire. Many interesting features of this system were demonstrated, such as sharp drops to zero transmission at certain values of the stub length, repeated periodically. In Ref. 4 the potential usefulness of such systems for transistor action was pointed out, in particular for multiple-stub configurations. In these the sharp drops become extended to forbidden bands. The calculations[4] were carried out using a finite-element Green's-function method. Very recently, some properties of similar devices have been studied experimentally.[8]

In a different vein, Ulloa, Castaño, and Kirczenow[9] have considered a linear array of mesoscopic potential wells separated by square potential barriers. Propagation through such an array also reveals an interesting structure of plateaus and resonances, which could form the basis for a quite different type of transistor action. Experiments with such geometries have also been undertaken.[10]

These two types of device have periodic structure and one can easily imagine other similar devices that can be disassembled into basic pieces connected in series. In this paper we solve the Schrödinger equation that describes the propagation of the electron by a mode-matching technique; this technique is especially adapted to such a serial structure. The wave function at each end of a device segment is described by its modal-expansion coefficients. A transfer matrix is then derived which relates the coefficients at one end to those at the other. The total transfer matrix that represents the electron wave propagation through the entire device is then just the product of the transfer matrices of the segments in order. This offers important advantages in comparison to other mode-matching techniques already applied to the quantum-wire problem.[1,5,7,11]

Primarily we have in mind rectangular geometry and square potentials. However, more realistic smooth potentials can be accommodated by cutting each device segment into small enough slices. We illustrate this by solving a Gaussian-barrier problem. Because of the simplicity and the constructive nature of our method, it can be implemented even on an IBM PC/AT computer and complete a typical calculation in about 10 min.

By combining features of the two above-mentioned examples, we propose a mesoscopic device with both sidearms and blocking bridges. This structure manifests both the quarter-wave mechanism and quantum tunneling effects, which are the operating principles of the above two devices, and thus has interesting physical properties that might be of interest for practical applications.

The paper is organized as follows. Section II introduces the method by solving the one-dimensional (1D)

mesoscopic-crystal problem, for which Sec. III contains some results. In Sec. IV we outline our solution for a quantum wire with a single stub, and with N stubs. Section V presents the results for the multiple-stub wire and Sec. VI discusses the proposed structure. The final section contains the conclusions and further remarks.

II. THE ONE-DIMENSIONAL MESOSCOPIC CRYSTAL

Recently, Ulloa, Castaño, and Kirczenow[9] have considered transport in a mesoscopic device formed by a linear array of mesoscopic potential wells separated by finite-height square potential barriers which can be created by a bridging mask over the semiconductor substrate. The device is illustrated in Fig. 1. We propose to call such a device a mesoscopic crystal. As is customary, we model the quantum wire as a two-dimensional waveguidelike device. The electron wave function satisfies the Schrödinger equation in a two-dimensional potential with infinitely repulsive walls. We label the width of the main wire to be a, and take the x axis to be parallel to the wave propagation direction. The device consists of $n+1$ bridge regions each of length d in which $V = V_0$, connected by segments of length l in which $V = 0$. For the moment, all segments have the same width a. Our model is identical to that of Ref. 9, except that we assume the entrance and exit leads at each end to be infinitely long, while the authors of Ref. 9 took them more realistically to have finite length. However, as can be seen from the results of our calculation, this makes very little difference. See also Ref. 12 for a discussion of this point.

We are going to solve the wave equation in the form

$$\nabla^2\phi + (E - V)\phi = 0, \tag{1}$$

where $E = 2\varepsilon m^*/\hbar^2$ is the energy in units Å^{-2}, m^* is the effective mass, and ε is the energy in eV. It is similar for the potential energies $V(x)$ and $v(x)$. Since the wire has uniform width and the potential depends only on the longitudinal coordinate x, one can separate variables: $\phi_n(x,y) = \psi(x)\sin(n\pi y/a)$, where $\psi(x)$ satisfies the one-dimensional Schrödinger equation

$$\psi''(x) + [E_{1d} - V(x)]\psi(x) = 0. \tag{2}$$

Here we have defined $E_{1d} = E - (n\pi/a)^2$. Solving the above equation, we find the conductance, $g(E_{1d}) = (2e^2/h)T$, for the one-dimensional system where T is the transmission probability. Then the conductance for the two-dimensional (2D) system is just

$$G(E) = \sum_{n\in\{\text{open}\}} g[E - (n\pi/a)^2]. \tag{3}$$

Here the notation ($n \in \{\text{open}\}$) stands for a sum over all propagating channels (those with $E_{1d} > 0$). To simplify the discussion, we write $E_0 = (\pi/a)^2$ for the threshold of the first propagating channel. Then one sees that the curve $G(E)$ is just the superposition of shifted curves $g(E_{1d})$: the first term is shifted by $E_0 = (\pi/a)^2$, the second one by 2^2E_0, the third by 3^2E_0, etc. Since $g(E_{1d})$ approaches unity when $E_{1d} \gg V$, in the large-energy region $G(E)$ will have a repeated steplike pattern. One example of this is shown in Fig. 2.

Knowing this relation between $G(E)$ and $g(E_{1d})$, we need only concentrate on 1D solutions. First we consider the propagation across a segment with $V = V_0$ and length d. As in Fig. 1 we represent this segment by a small rectangle with two leads, with left-end coordinate x_1 and right-end x_2. The potential in the external leads is zero, but one can easily adopt a different value if desired. We express the wave function in the two leads as

$$\psi_k(x) = c_k \exp[i\alpha(x - x_k)] + \bar{c_k}\exp[-i\alpha(x - x_k)], \tag{4}$$

where the wave number is $\alpha = \sqrt{E_{1d}}$. The internal wave function can be expressed as

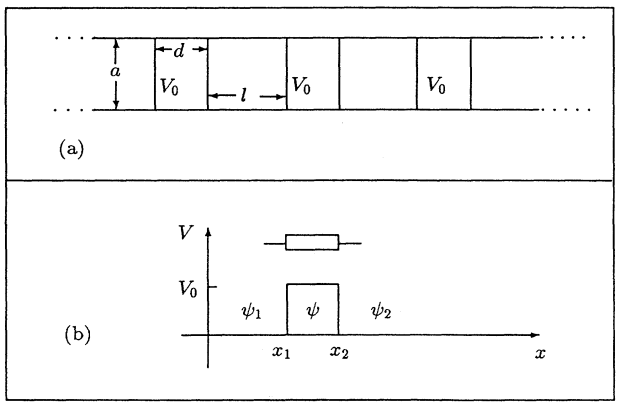

FIG. 1. (a) The structure of a one-dimensional mesoscopic crystal. The electrons are confined between the two horizontal lines and experience a periodic blocking potential in the regions marked $V = V_0$. The potential elsewhere is zero. The entrance and exit leads at each end are considered to be infinitely long. (b) The bridge considered as a segment of the device.

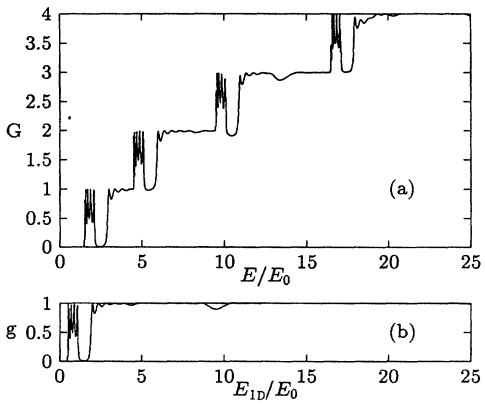

FIG. 2. (a) Steplike repeating structure of the conductance in the 1D mesoscopic crystal with five cells. The parameters are $d = l = 0.5a$, $V_0 = E_0$. (b) The underlying 1D conductance of part (a).

$$\psi(x) = f\exp[i\gamma(x - x_1)] + \bar{f}\exp[-i\gamma(x - x_1)], \quad (5)$$

where $\gamma = \sqrt{E_{1d} - V_0}$. By matching the wave function and its derivative at each end, one finds

$$\begin{pmatrix} c_1^+ \\ c_1^- \end{pmatrix} = M \begin{pmatrix} c_2^+ \\ c_2^- \end{pmatrix}, \quad (6)$$

where

$$M = \begin{pmatrix} \cos(\gamma d) & -i\alpha/\gamma \sin(\gamma d) \\ -i\gamma/\alpha \sin(\gamma d) & \cos(\gamma d) \end{pmatrix} \quad (7)$$

and

$$c_k^+ = c_k + \bar{c}_k \quad c_k^- = c_k - \bar{c}_k. \quad (8)$$

Thus if we regard the vector $\{c_k^+, c_k^-\}$ as representing the wave function at a particular point, the transfer matrix M takes us from the right side to the left side of a particular bridge section. In addition, if we set $V_0 = 0$ and $d = l$, we have the appropriate transfer matrix for a zero potential connecting segment:

$$P = \begin{pmatrix} \cos(\alpha l) & -i\sin(\alpha l) \\ -i\sin(\alpha l) & \cos(\alpha l) \end{pmatrix}. \quad (9)$$

The total transfer matrix for the whole device with $n+1$ bridges is then

$$M^{\text{total}} = (MP)^n M. \quad (10)$$

To compute the conductance for this system we must apply physical boundary conditions. Suppose the wave travels from left to right, with $\{c_{\text{in}}^+, c_{\text{in}}^-\}$ and $\{c_{\text{out}}^+, c_{\text{out}}^-\}$ representing the entrance and exit amplitudes, respectively. Since there is no backward wave at the right exit, we have $\bar{c}_{\text{out}} = 0$, which implies $c_{\text{out}}^+ = c_{\text{out}}^- = c_{\text{out}}$. From this, one finds

$$2c_{\text{in}} = \left(\sum_{i,j=1}^{2} M_{i,j}^{\text{total}} \right) c_{\text{out}}. \quad (11)$$

Since this is a one-dimensional system, $g = T = |c_{\text{out}}/c_{\text{in}}|^2$ in units of $2e^2/h$; thus

$$g = \left| \frac{2}{\sum_{i,j=1}^{2} M_{i,j}^{\text{total}}} \right|^2. \quad (12)$$

Although the model we have just solved is particularly simple, it demonstrates a general approach for dealing with any serially connected device, which we will apply later in this paper: (1) disassemble the device into its basic building blocks; (2) find the transfer matrix for each building block by matching the wave function and its derivative inside the block with the two leads; (3) compute the total transfer matrix by multiplying the transfer matrices for each segment of the device in order; (4) apply physical boundary conditions to determine the actual solution.

III. RESULTS FOR THE ONE-DIMENSIONAL MESOSCOPIC CRYSTAL

The discussion in the preceding section, relating the behaviour of $G(E)$ to that of the one-dimensional conductance, makes the calculations very straightforward and allows an easy interpretation of the roles of the different parameters defining the device. To stress this further we show in Fig. 2 the one-dimensional and total conductances for a device with $n = 5$ wells as a function of energy, for typical values of the other parameters. It is clear that all the features of the one-dimensional plot appear periodically and are clearly separated in the successive steps of $G(E)$.

The structure of the 1D conductance exhibits well-known universal features that have a very simple interpretation. At low energies the conductance is always close to zero except for resonant peaks that correspond to transmission by tunneling through the quasi-bound-states of the system. Their energies can be estimated by considering a system with the same n wells but such that in the entrance and exit leads, the potential, instead of dropping to zero, remains constant and equal to V_0 up to infinity. The bound states of this modified system correspond then to the well-known minibands. For the simplest case, that of a single square well, the energy of the lowest state can be accurately computed using the analytic approximation given in Ref. 13. For the case of two square wells, in the limit when V_0 is very large, two degenerate orthogonal states can be formed. One may regard these as placing the particle in either of the wells, or alternatively as the symmetric and antisymmetric linear combinations. When V_0 is decreased the symmetric and antisymmetric wave functions split in energy due to the different matching requirements in the midpoint between the wells, and as V_0 tends to zero this splitting increases towards the value corresponding to the separation of the first and second bound states of the single wider well.

The same qualitative features apply also in the case of n wells, the first being that the number of peaks equals the number of wells. Furthermore, in Figs. 3(a) and 3(b) we compare the cases $V_0 = 1$ and 2: increasing V_0 decreases the width of the miniband. This is in agreement with the above discussion, and moreover, since the height of the repulsive barrier increases, the average energy of all these states is pushed up. In Figs. 3(a) and 3(c) the same effects are seen when the width of the bridges increases: for the lowest states the increase in the effective repulsion (d^2V_0) overwhelms the previous effect and the energies increase, whereas for the highest it is the opposite, and the result is that the width of the miniband decreases. In addition, one notices in both cases shown in Fig. 3 that, when the height or the width of the barriers decreases, the widths of the resonant peaks increase.

When the Fermi energy is further increased the figures show that the transmission drops to zero, defining a forbidden band, until tunneling is replaced by transmission over the barrier and g_{1d} rises towards unity. The energy at which this rise takes place is independent of n and is determined by the barrier height. [For a single square barrier, the resonant energies, for which $T = 1$,

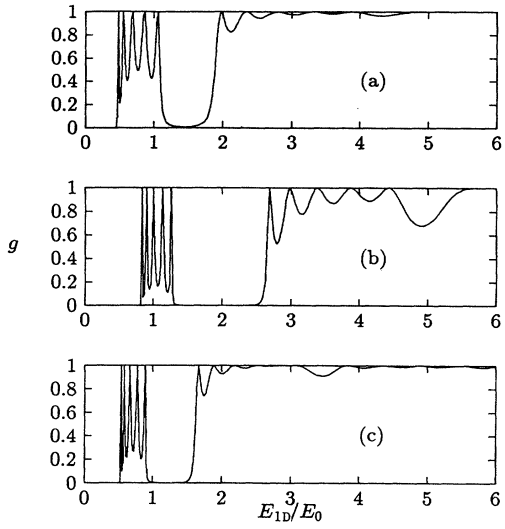

FIG. 3. Dependence on barrier height and width, $n = 5$, $l = 0.5a$: (a) $V_0 = E_0$, $d = 0.5a$ as in Fig. 2; (b) $V_0 = 2E_0$, $d = 0.5a$; (c) $V_0 = E_0$, $d = a/\sqrt{2}$.

are $E_R = V_0 + (\hbar^2/2m)(k\pi/d)^2$.] But, as shown in Fig. 4 the rise becomes steeper as the number of wells in the device increases (we compare cases with $n = 3$ and 50). The case $n = 50$ shown in the figure has been chosen to illustrate the computational accuracy of our method. Experiments using devices with such a large number of bridges are currently being considered.[10]

In reality, the potential barrier generated by gate bridges will not be a perfect step function. The exact form of the potential "felt" by the electron will depend on accidents of fabrication, and one will never have a precise description of it. In order to see whether the detailed shape of this potential affects the device behavior, we consider an alternative barrier shape. One can assume that the potential will be peaked about the center of each strip, so a Gaussian shape is a reasonable form to try. To calculate the conductance in a model with

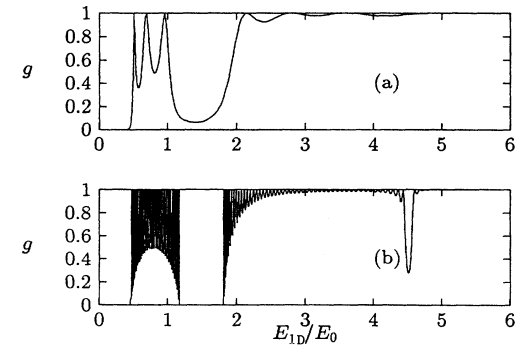

FIG. 4. Dependence on the number of periods, $l = d = 0.5a$, $V_0 = E_0$: (a) $n = 3$; (b) $n = 50$.

arbitrary x dependence, we can still utilize the formulas developed for the step-function potential. The basic problem is to find the transfer matrix for a single period. We divide this single period into slices small enough so that the potential in each piece may be considered to be constant. Thus we replace an arbitrary smooth function by a sequence of step functions. Explicitly,

$$M^{\text{total}} = M_s^{n+1}, \tag{13}$$

$$M_s = \prod_k \begin{pmatrix} \cos(\gamma_k \delta x_k) & -i\alpha/\gamma_k \sin(\gamma_k \delta x_k) \\ -i\gamma_k/\alpha \sin(\gamma_k \delta x_k) & \cos(\gamma_k \delta x_k) \end{pmatrix}, \tag{14}$$

where γ_k is the average γ value in a given slice k and δx_k is the length of the slice. We write the Gaussian potential in the form $V = \eta V_0 \exp(-x^2/\sigma^2)$, with x measured from the center of the bridge. We choose parameters so that the integral of $xV(x)$ over a half-period is the same as for the square barrier, with η larger than 1, in order to have similar heights and widths of the two potentials, as seen in the inset to Fig. 5. In our calculation, 100 slices have been used to simulate the Gaussian potential. The two barriers are compared in Fig. 5, where the one-dimensional conductances for typical values of the parameters are shown, and remarkable agreement is seen. We conclude that smooth deviations in the shape of the potential from that of a square barrier do not lead to important changes in the conductance.

It is possible also to design experiments[10] in which the blocking bridges are connected in two groups, the bridges at even numbered positions given one potential and the odd ones a different potential. Our formulation is also easily adapted to this configuration. As could be expected, we find that when the two potentials are close, the device's behavior is very similar to that of the single potential case. When the difference between the potentials becomes large, the device's behavior is determined by the stronger set of potential barriers. The weaker set of barriers can then be ignored.

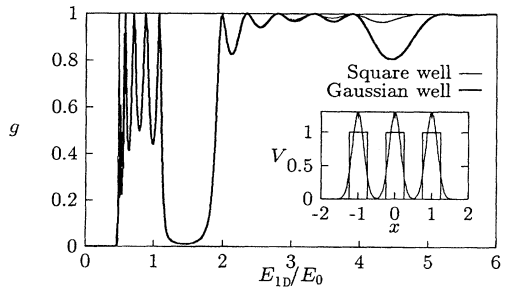

FIG. 5. Comparison of conductances for a Gaussian and a square barrier, $n = 5$, period $= a$. Light line: square well with $V = V_0$ and $d = 0.5a$ as in Fig. 2. Dark line: Gaussian potential $V = 1.3V_0 \exp(-x^2/0.22^2)$. The integral of $xV(x)$ over a half period is kept the same for both cases. Inset: Three-period potential structure for Gaussian and square wells.

IV. THE MULTIPLE-STUB QUANTUM-WIRE PROBLEM

The general structure of a multiple-stub quantum wire is sketched in Fig. 6. The main part of the device is a uniform wire of width a, on either side of which there are a number of arms (stubs), whose lengths are effectively defined by control signals applied at their ends. We label the width of the jth stub as b_j and its length $c_j - a$. The distances between adjacent arms are $l_{j,j+1}$.

The basic building block of a multiple-stub wire is a simple T-shaped device with a single stub, as shown in Fig. 7, and we require its transfer matrix first. Following the notation of Sec. II, the regions (1) and (2) are the leads of the device segment.

Inside the leads, since the wave function must vanish on the walls, the y dependence must be $\sin(n\pi y/a)$, where the various values of n define reaction channels. In order to satisfy the differential equation (1), with $V = 0$ everywhere, we write

$$\phi_1 = \sum_n (c_{1n} e^{i\alpha_n x} + \bar{c}_{1n} e^{-i\alpha_n x}) \sin \frac{n\pi y}{a} \quad . \tag{15}$$

Similarly,

$$\phi_2 = \sum_n (c_{2n} e^{i\alpha_n (x-b)} + \bar{c}_{2n} e^{-i\alpha_n (x-b)}) \sin \frac{n\pi y}{a} \quad , \tag{16}$$

where the wave number for channel n is

$$\alpha_n = \sqrt{E - (n\pi/a)^2} \quad . \tag{17}$$

For an open (closed) channel α_n is real (pure imaginary).

In the internal region, ϕ must vanish at $y = 0$ and c; thus the basic y dependence is $\sin(m\pi y/c)$. However, the internal wave function should also vanish at each side of the arm outside the main wire and smoothly connect to the external wave function along lines OA and BC ($x = 0$ and $x = b$). We first construct two auxiliary sets of solutions to the wave equation, one of which matches the wire on the left, and the other, the wire on the right, with each vanishing elsewhere on the boundary. This is a procedure first introduced by Kühn.[14] The appropriate boundary conditions are

$$\chi_{k0}(x = b, y) = 0,$$
$$\chi_{k0}(x = 0, y) = \begin{cases} 0, & y > a \\ \sin(k\pi y/a), & y \le a \end{cases} \tag{18}$$

$$\chi_{0k}(x = 0, y) = 0,$$
$$\chi_{0k}(x = b, y) = \begin{cases} 0, & y > a \\ \sin(k\pi y/a), & y \le a. \end{cases} \tag{19}$$

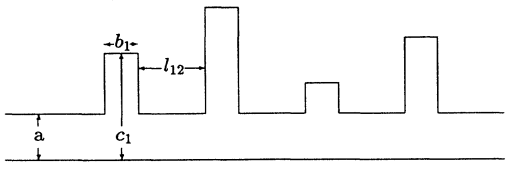

FIG. 6. Structure of an n-stub quantum wire.

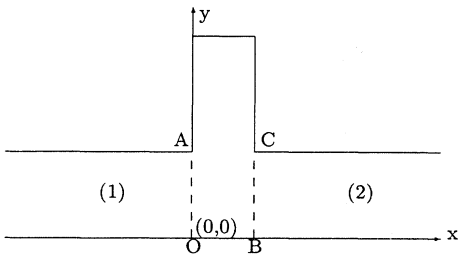

FIG. 7. Structure of a single-stub quantum wire.

The solutions χ_{0k} are expanded as

$$\chi_{0k} = \sum_m [u_m \sin(\gamma_m x) + v_m \cos(\gamma_m x)] \sin \frac{m\pi y}{c}, \tag{20}$$

where the wave number in the internal region is

$$\gamma_m = \sqrt{E - (m\pi/c)^2} \quad . \tag{21}$$

The boundary condition at $x = 0$ requires that $v_m = 0$, whereas the condition at $x = b$ gives

$$\sum_m u_m \sin(\gamma_m b) \sin(m\pi y/c) = \begin{cases} 0, & y > a \\ \sin(k\pi y/a), & y \le a. \end{cases} \tag{22}$$

This is a Fourier expansion whose coefficients are

$$u_m = \frac{2}{c} \frac{I_{km}}{\sin(\gamma_m b)}, \tag{23}$$

where

$$I_{nm} = \int_0^a \sin\left(\frac{n\pi y}{a}\right) \sin\left(\frac{m\pi y}{c}\right) dy$$
$$= \frac{a}{2\pi} \left(\frac{\sin \pi(n - ma/c)}{n - ma/c} - \frac{\sin \pi(n + ma/c)}{n + ma/c} \right), \tag{24}$$

giving

$$\chi_{0k} = \frac{2}{c} \sum_m \frac{\sin(\gamma_m x)}{\sin(\gamma_m b)} I_{km} \sin \frac{m\pi y}{c}. \tag{25}$$

Similarly,

$$\chi_{k0} = \frac{2}{c} \sum_m \frac{\sin[\gamma_m (b - x)]}{\sin(\gamma_m b)} I_{km} \sin \frac{m\pi y}{c}. \tag{26}$$

The actual wave function in the internal region can be expanded in terms of these auxiliary solutions χ_{0k} and χ_{k0}:

$$\phi = \sum_k (f_k \chi_{k0} + \bar{f}_k \chi_{0k}) \quad . \tag{27}$$

The continuity of the wave function at $x = 0$ and b requires that $f_k = c_{1k} + \bar{c}_{1k}$ and $\bar{f}_k = c_{2k} + \bar{c}_{2k}$, thus

$$\phi = \frac{2}{c}\sum_{km} \frac{(c_{1k}+\bar{c}_{1k})\sin[\gamma_m(x-b)] + (c_{2k}+\bar{c}_{2k})\sin(\gamma_m x)}{\sin(\gamma_m b)} I_{km} \sin\frac{m\pi y}{c}. \tag{28}$$

Similarly, matching the derivative ϕ' at $x = 0$ gives

$$\sum_n (c_{1n}-\bar{c}_{1n}) i\alpha_n \sin\frac{n\pi y}{a} = \frac{2}{c}\sum_{km} \frac{(c_{2k}+\bar{c}_{2k}) - (c_{1k}+\bar{c}_{1k})\cos(\gamma_m b)}{\sin(\gamma_m b)} \gamma_m I_{km} \sin\frac{m\pi y}{c}, \tag{29}$$

and at $x = b$,

$$\sum_n (c_{2n}-\bar{c}_{2n}) i\alpha_n \sin\frac{n\pi y}{a} = \frac{2}{c}\sum_{km} \frac{(c_{2k}+\bar{c}_{2k})\cos\gamma_m b - (c_{1k}+\bar{c}_{1k})}{\sin\gamma_m b} \gamma_m I_{km} \sin\frac{m\pi y}{c}. \tag{30}$$

Multiplying by $\sin(l\pi y/a)$ on both sides of the above two equations and integrating from zero to a yields

$$(c_{1n}-\bar{c}_{1n}) i\alpha_n = \frac{4}{ac}\sum_{km} \frac{(c_{2k}+\bar{c}_{2k}) - (c_{1k}+\bar{c}_{1k})\cos(\gamma_m b)}{\sin(\gamma_m b)} \gamma_m I_{nm} I_{km} \tag{31}$$

and

$$(c_{2n}-\bar{c}_{2n}) i\alpha_n = \frac{4}{ac}\sum_{km} \frac{(c_{2k}+\bar{c}_{2k})\cos(\gamma_m b) - (c_{1k}+\bar{c}_{1k})}{\sin(\gamma_m b)} \gamma_m I_{nm} I_{km}. \tag{32}$$

To simplify these relations, we again use Eq. (8). Define matrices A, B, and α whose elements are

$$A_{nk} = \frac{4}{ac}\sum_m \frac{\gamma_m}{\sin(\gamma_m b)} I_{nm} I_{km}, \tag{33}$$

$$B_{nk} = \frac{4}{ac}\sum_m \gamma_m \cot(\gamma_m b) I_{nm} I_{km}, \tag{34}$$

$$\alpha_{nk} = \alpha_n \delta_{nk}, \tag{35}$$

and column vectors C_i^-, C_i^+, whose elements are c_{ik}^-,c_{ik}^+, respectively. In this notation, we have

$$i\alpha C_1^- = AC_2^+ - BC_1^+, \tag{36}$$

$$i\alpha C_2^- = BC_2^+ - AC_1^+, \tag{37}$$

where A and B are real-valued matrices. These two equations determine C_1^+ and C_1^- in terms of C_2^+ and C_2^-. The resulting transfer matrix is

$$M = \begin{pmatrix} 1 & 0 \\ 0 & -i\alpha^{-1} \end{pmatrix} \begin{pmatrix} A^{-1}B & -A^{-1} \\ A - BA^{-1}B & BA^{-1} \end{pmatrix} \begin{pmatrix} 1 & 0 \\ 0 & i\alpha \end{pmatrix}, \tag{38}$$

so that

$$M_{11} = A^{-1}B, \quad M_{12} = -iA^{-1}\alpha, \tag{39}$$

$$M_{21} = -i\alpha^{-1}(A - BM_{11}), \quad M_{22} = i\alpha^{-1}BM_{12}. \tag{40}$$

This transfer matrix relates the incoming to the outgoing wave across the stub for arbitrary initial conditions.

The other building block of a multiple-stub wire is a simple straight wire segment. Just as in Sec. II, the transfer matrix induced by the part connecting the ith and jth stub is simply

$$P(ij) = \begin{pmatrix} \cos(\alpha l_{ij}) & -i\sin(\alpha l_{ij}) \\ -i\sin(\alpha l_{ij}) & \cos(\alpha l_{ij}) \end{pmatrix}. \tag{41}$$

The difference between this and Eq. (9) is that α is now a diagonal matrix. Given M and P, the total transfer matrix for an n-stub quantum wire is

$$M^{\text{total}} = \prod_{i=1}^{n-1} [M(i)P(i,i+1)]M(n). \tag{42}$$

Suppose the wave function at the entrance of the first stub is represented by $\{C_{\text{in}}^+, C_{\text{in}}^-\}$ and at the exit of the last stub by $\{C_{\text{out}}^+, C_{\text{out}}^-\}$. Then

$$\begin{pmatrix} C_{\text{in}}^+ \\ C_{\text{in}}^- \end{pmatrix} = M \begin{pmatrix} C_{\text{out}}^+ \\ C_{\text{out}}^- \end{pmatrix}. \tag{43}$$

We now discuss the physical conditions imposed on the ingoing and outgoing wave components. Depending on energy, α_n could be real or pure imaginary. We choose α_n to be positive for an open channel and lying on the positive imaginary axis for a closed channel. With this choice, $\bar{c}_{\text{out},n}$ represents either a leftward moving wave or an exponentially divergent wave at positive infinity. Now, for the sake of argument we will take the incident wave to come from the left; in this situation, we must set $\bar{C}_{\text{out}} = 0$ and thus $C_{\text{out}}^+ = C_{\text{out}}^- = C_{\text{out}}$. Physically $c_{\text{out},n}$ represents the transmitted wave component in channel n. In the device entrance region, components $\bar{c}_{\text{in},n}$ are allowed. When α_n is real, $\bar{c}_{\text{in},n}$ represents the amplitude of the reflected wave in channel n. For a closed channel, the reflected wave is a transient that decays exponentially. For open channels, $c_{\text{in},n}$ represents the incoming wave amplitude in channel n. For closed channels, $c_{\text{in},n}$ must vanish in order to avoid divergence at negative infinity. Explicitly,

$$C_{\text{in}}^+ = C_{\text{in}} + \bar{C}_{\text{in}} = M_{11}^{\text{total}} C_{\text{out}} + M_{12}^{\text{total}} C_{\text{out}}, \tag{44}$$

$$C_{\text{in}}^- = C_{\text{in}} - \bar{C}_{\text{in}} = M_{21}^{\text{total}} C_{\text{out}} + M_{22}^{\text{total}} C_{\text{out}}, \tag{45}$$

where M_{ij}^{total} are blockwise submatrices of M^{total}.

Adding these two equations, we can determine the transmitted amplitudes C_{out} by solving

$$\left(\sum_{ij} M_{ij}\right) C_{\text{out}} = 2C_{\text{in}}. \tag{46}$$

Following this, the reflection coefficients are given by

$$\bar{C}_{\text{in}} = \tfrac{1}{2}(M_{11} + M_{12} - M_{21} - M_{22})C_{\text{out}} \quad . \tag{47}$$

The total transmission and reflection coefficients are then given by

$$T = \frac{\sum_{n\in\{\text{open}\}} c_{\text{out},n} c^*_{\text{out},n} \alpha_n}{\sum_{n\in\{\text{open}\}} c_{\text{in},n} c^*_{\text{in},n} \alpha_n} \tag{48}$$

and

$$R = \frac{\sum_{n\in\{\text{open}\}} \bar{c}_{\text{in},n} \bar{c}^*_{\text{in},n} \alpha_n}{\sum_{n\in\{\text{open}\}} c_{\text{in},n} c^*_{\text{in},n} \alpha_n}. \tag{49}$$

For completeness, we mention that for the bound-state calculation, one must solve the homogeneous version of Eq. (46) with $C_{\text{in}} = 0$.

We also emphasize that in our formalism, once we know how to handle the single-stub case, the multiple-stub problem can be solved with little additional labor. This is not so for either the recursive Green's-function method or the usual mode-matching approach.

V. RESULTS FOR THE MULTIPLE-STUB QUANTUM WIRE

In Fig. 8 we show the transmission coefficient for the single-stub case in its fundamental mode, as a function of the effective stub length c, for three given energies. This reproduces in detail the results presented in Ref. 4. Notice that because of the high resolution of our calculation, the sharp drops of the curve at $\varepsilon - \varepsilon_0 = 0.199$ eV are fully explored (ε_0 is the fundamental mode energy in eV).

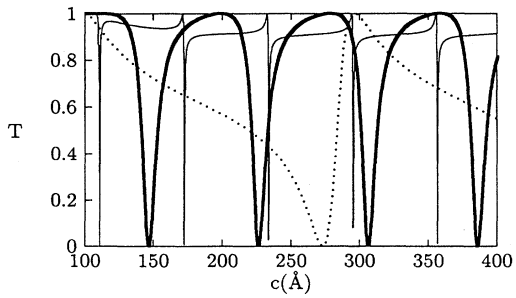

FIG. 8. Transmission versus stub length c for a single-stub configuration, reproducing Fig. 2(b) of Sols *et al.* (Ref. 3). $a = b = 100$ Å, $m^* = 0.05$. The energies given are $\varepsilon - \varepsilon_0 = 0.02$ eV (dotted line), 0.118 eV (heavy line), and 0.199 eV (light line).

Some further insight into the solution is provided by drawing the electron probability density ($|\phi|^2$), as in Fig. 9. In these figures the electron is incident from the upper right. Away from the stub, the intensity would be uniform, and of sinusoidal shape across the main wire. Figures 9(a)–9(d) show cases in the sequence $T = 0, 1, 0, 1$ starting from the first zero, as shown in Fig. 8, with $\varepsilon - \varepsilon_0 = 0.118$ eV. The corresponding c values are 146, 200, 226, and 280 Å. Notice that from one zero to the next [Figs. 9(a) and 9(c)], or from one maximum to the next [Figs. 9(b) and 9(d)], the stub length c has only to be increased so as to accommodate an additional half-wavelength. Aside from this additional half-wavelength in the top of the stub, nothing else changes. Thus it is evident that the $T = T(c)$ curve is a periodic function with period

$$\delta c = \pi/\sqrt{E - (\pi/b)^2}. \tag{50}$$

These electron-density plots give us the following physical picture: the electron wave propagates along the stub direction with wave number $\sqrt{E - (\pi/b)^2}$ and is reflected back, thus creating a standing wave inside the stub. Near the edge of the stub, the wave reflected from the stub couples to the wave in the main wire. When the phase shift between the two is $2n\pi$, they reinforce each other to give $T = 1$, and when it is $(2n+1)\pi$, one obtains $T = 0$. Unfortunately, it is not easy to estimate the position where

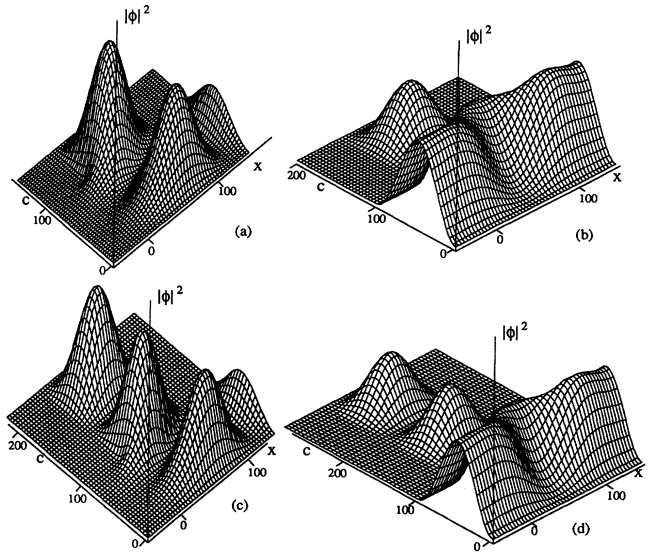

FIG. 9. Visualization of the electron current in a single-stub configuration; the geometrical parameters are the same as in Fig. 8. The energy is at $\varepsilon - \varepsilon_0 = 0.118$ eV. $m^* = 0.05$. (a) $T = 0$, $c = 146$ Å; (b) $T = 1$, $c = 200$ Å; (c) $T = 0$, $c = 226$ Å; (d) $T = 1$, $c = 280$ Å. (c) has an additional half-wavelength in the stub compared to (a), and (d) has an additional half-wavelength compared to (b).

the coupling takes place. However, our expression for the period δc is independent of this position and thus it matches the exact result very well. The principle discussed here is well known in waveguide physics and is called the quarter-wave mechanism.

In Fig. 10 we show the transmission for the case of five stubs. As already discussed in Ref. 4, the most favorable situation is to choose the stubs to be of the same width as the main wire. To avoid having too many parameters, we choose all stubs to be of equal length. As is familiar from waveguides, the sharp minima in T become extended, in the multiple-stub case, into bands over which the transmission is blocked. For a practical device, this will be a much more useful situation, as it will not require an extremely precise tuning of the stub length. Meanwhile the drop in conductance becomes very sharp. Although the width of the blocked region increases as more stubs are added, it does not change much after five. This broadening of the valleys of the $T = T_n(c)$ curve for the multiple-stub case can be understood by raising the $T = T_1(c)$ curve for the single-stub case, to a power, $T_n(c) \approx [T_1(c)]^n$.

Although the multiple-stub scheme is a systematic way to get minimum conductance over a broader range of stub lengths, there are nevertheless other ways. Figure 11 shows the single-stub wire operating at an energy above the threshold of the second mode. In general, when different modes interfere the output will be more complicated than in the single-mode case. As shown in the figure, one can have a rather squarish pattern of maxima and minima, and the conductance change is still one unit. However, we lose the ability of totally blocking the wire.

To end this section, we mention some potential difficulties of our method. Equation (38) requires the inverse of the matrix A. We found that A becomes numerically singular when too many closed channels are included in the calculation. However, in practice, the amplitudes of closed channels decrease very fast, which allows one to consider only a few of them in the calculation. The fact that our calculation agrees with that of Sols *et al.* can be taken as a justification of our method. We have also compared our results against those of the usual mode-matching method and found good agreement. An extension of our method to a more general situation and a systematic way of constructing linear equations in the conventional mode-matching method will be presented elsewhere.

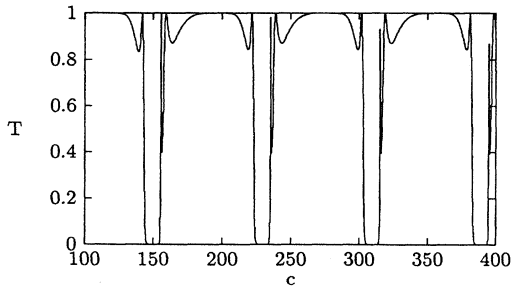

FIG. 10. Transmission coefficient vs stub length for a five-stub wire. $a = d = l = 100$ Å, $\varepsilon - \varepsilon_0 = 0.118$ eV, $m^* = 0.05$.

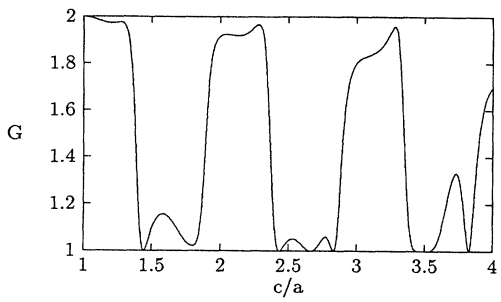

FIG. 11. Conductance of a single-stub wire at high energy. $E/E_0 = 5.2$, $b = a$.

VI. MULTIPLE-STUB WIRE WITH BLOCKING BRIDGES

In the previous sections we have discussed two systems, the 1D mesoscopic-crystal and the multiple-stub wire. In this section, we combine them in a single mesoscopic system. This is very easy to realize, at least theoretically. If you have already made a 1D mesoscopic crystal, you add stubs to the side of each well; if what you have is a multiple-stub wire, then you add blocking bridges on the main wire connecting stubs as well as on the two entrances. Experimentally, devices such as the "corrugated channel" considered by van Kouwenhoven *et al.*[8] are precisely of this kind, although as discussed by those authors the detailed shape of the "saddle-shaped potential in the narrow regions" is not known. Here we are going to assume that both the stub length and the width and height of the blocking potential can be changed independently through some effective control voltages applied to appropriately designed gates, to explore the effects of these changes on the device response. We have already shown in the case of the 1D mesoscopic crystal that these two parameters are the most relevant in determining that response. A word on notation: we will use n to represent the number of stubs, so that $n+1$ is the number of blocking bridges. The meanings of b, c, and d are the same as before . The distance from the edge of the bridge to the entrance of the nearby stub will be s.

Since we know how to compute the transfer matrix for a bridge, for a plain wire and for a stub, there is no need to go into detail for the solution of this device. Instead, we jump directly to a discussion of some results. First, as we have emphasized in Sec. II, the 1D mesoscopic crystal is strictly a one-dimensional problem, despite its 2D appearance. It is interesting to see how the change of stub length affects this mode-decoupling feature. Figure 12 shows the results of the calculation with very short stubs. The device is identical to that used to generate Fig. 2(a), except that five stubs with $b = 0.5a$, $c = 1.1a$ are added. By comparing with Fig. 2(a), we see big differences, despite the fact that the stubs are only $0.1a$ long. We see virtually no difference when the energy is below the second mode. As the energy goes up, more and more channels open and greater differences appear. First of all the peaks due to resonant tunneling

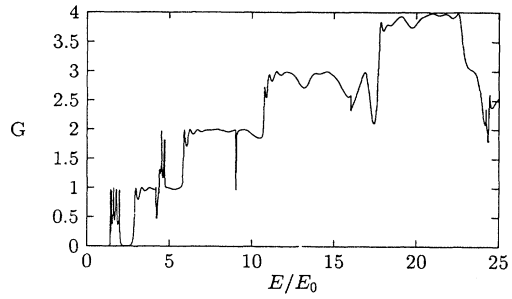

FIG. 12. Conductance of a 1D mesoscopic crystal with small stubs. $n = 5$, $b = d = 0.5a$, $s = 0$, $c = 1.1a$

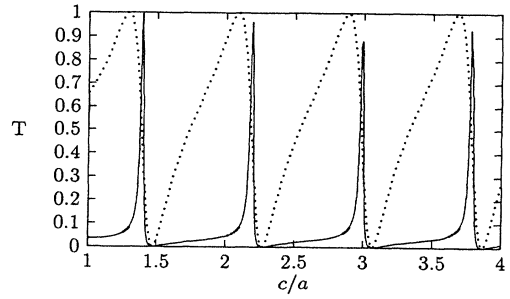

FIG. 13. Transmission coefficient of a single-stub wire with two blocking bridges. $b = a$, $s = 0.25a$, $d = 0.5a$, $E = 2.57E_0$. Solid line: $V_0 = 2E_0$; dotted line: $V_0 = E_0$.

disappear, and although one can still see the steplike increases in G at the same energies, they become more and more obscured by apparently random fluctuations whose width and amplitude tend to increase with energy. This could possibly explain the results quoted by van Kouwenhoven *et al.*[8] for their multiple-stub (15 fingers) device in the zero-magnetic-field case: they found "no evidence for the formation of a band structure and for quantized plateaus in G resulting from the transverse confinement." Furthermore, it can be expected that working at finite temperatures will smooth out further the remaining oscillations in G, due to transmission above the barriers, and lead to a rather smoothly increasing conductance with little trace of the quantal effects so clearly seen in Fig. 2(a). As the energy increases, the conductance will, however, show appreciable fluctuations, seemingly random, due to interfering effects of different transverse channels. (Examples of these are clearly seen in Fig. 12 in the interval $12 < E/E_0 < 18$ and in the strong drop at $E/E_0 \approx 22$.) We believe that even small stubs will greatly mix the high-energy modes whose wavelengths become small in comparison to other geometrical length scales of the problem. This implies that the width of a 1D mesoscopic-crystal should be kept very uniform if one is to see channel decoupling take place.

Guided by the above results we consider now in detail the behavior of the device in the low-energy region, when only one transverse mode is allowed, and study the transmission when both the blocking potential and the stubs exert their full effect. When the blocking potential is higher than the electron kinetic energy (as we have mentioned in Sec. III) the device is basically shut off, except at those energies where resonant tunneling takes place. In our combined structure, the resonant cavity can be controlled by changing the effective stub length. Figure 13 shows the transmission coefficients for a single-stub wire with a blocking bridge at each end. Without bridges, the $T = T(c)$ curve is identical to the dark line in Fig. 8. When raising V_0 to E_0 and $2E_0$, we found that the minima do not move; they remain in the positions determined by the single-stub wire without bridges. Furthermore, these minima do not move even when s varies. This shows that the minima are determined only by the coupling of the main wire to the stub. It is the standing wave in the stub that determines the period of the $T = T(c)$ curve. Unlike the minima, the maxima do move when either the blocking potential or s changes. This is clearly because the maxima are resonant peaks when V_0 is not too small. The effective resonant cavity is the part of the main wire sandwiched between the two bridges and the part of the stub from the entrance to the first node of the standing wave. Thus if c_1 gives a maximum, so must $c_1 + \delta c$, where δc is given by Eq. (50). Thus we see that the number of maxima equals the number of minima, and that they have the same period. However, the spacing between adjacent maxima and minima is another story. From this discussion, we see that both the quarter-wave and quantum-resonant-tunneling mechanisms are effective in this combined structure. Practically, because we have greater controllability over this device, we may think of using the stub length as the main control to realize transistor action, and the voltage applied to the bridges as a dynamical parameter to change the device characteristics. Returning to Fig. 13, we see how V_0 can greatly change the function $T = T(c)$. Think about the case $V_0 = 0$, where the device is basically open, and only cut off at certain specific c values. But when $V_0 = 2E_0$, the situation is almost the reverse, and the device is basically a closed one, opening only when c causes resonant behavior.

To conclude this section, we introduce the last figure in this paper. Figure 14 shows a five-stub wire with six

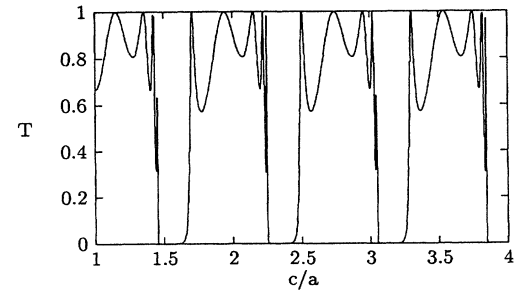

FIG. 14. Transmission coefficient of a five-stub wire with six blocking bridges. $b = a$, $s = 0.25a$, $d = 0.5a$, $E = 2.57E_0$, $V_0 = E_0$.

bridges at potential $V_0 = E_0$; other relevant parameters remain unchanged from Fig. 13. As expected, the addition of the stub introduces more resonant peaks, and the number of peaks in one period is equal to the number of stubs, or the number of resonant cavities. This feature is passed along from the 1D mesoscopic-crystal model. However, the difference is that in this structure, these multiple peaks are observed through scanning the control signal on the stub. Further discussion of this combined structure will be presented elsewhere.

VII. SUMMARY AND REMARKS

We have presented a simple and efficient way of solving the electron-wave-propagation problem for serially connected quantum-wire devices. With this method, we have discussed several recently considered mesoscopic structures. We have emphasized the underlying principles governing the simplest of these structures: the quarter-wave mechanism for the single-sidearm wire and quantum tunneling effects for the 1D mesoscopic crystal. The interplay of these two effects can be seen in our combined structure, a quantum wire with both sidearms and blocking bridges as control gates. The structure has greater control capabilities.

ACKNOWLEDGMENTS

We are grateful to NSERC Canada for continuing support under operating Grant No. A-3198 (D.W.L.S. and H.W.). The work of J.M. was partially supported by Grant No. PB-87-0311 from DGICYT Spain and by the French-Spanish Exchange Program Grant No. 75/1990. In addition, D.W.L.S. is grateful to the Deutsche Forschungs Gemeinschaft and NSERC for support under the exchange program with Canada, and to Professor H. Arenhövel for the pleasant working conditions of the Institut für Kernphysik der Universtät Mainz, where some of this work was performed. Division de Physique Théorique is a unité de recherche des Universités Paris 6 et Paris 11, associée au CNRS.

---

*Permanent address: Department of Physics and Astronomy, McMaster University, Hamilton, Ontario, Canada L8S 4M1.

[1] S. Datta, Superlatt. Microstruct. **6**, 83 (1989).
[2] S. Datta, in *Physics of Quantum Electron Devices*, edited by F. Cappaso, Springer Series in Electronics and Photonics Vol. 28 (Springer, Berlin, 1990), pp. 321–352.
[3] F. Sols, M. Macucci, U. Ravaioli, and K. Hess, Appl. Phys. Lett. **54**, 350 (1989).
[4] F. Sols, M. Macucci, U. Ravaioli, and K. Hess, J. Appl. Phys. **66**, 3892 (1989).
[5] A. Weisshaar, J. Lary, S.M. Goodnick, and V.K. Tripathi, Appl. Phys. Lett. **55**, 2114 (1989).
[6] Y. Avishai and Y. B. Band, Phys. Rev. B **41**, 3253 (1990); Y. Avishai, M. Kaveh, and Y.B. Band, *ibid.* **42**, 5867 (1990).
[7] J. Martorell, S. Klarsfeld, D. W. L. Sprung, and Hua Wu, Solid State Commun. **78**, 13 (1991).
[8] L. P. van Kouwenhoven , F. W. J. Hekking, B. J. van Wees, C. J. P. M. Harmans, C. E. Timmering, and C. T. Foxon, Phys. Rev. Lett. **65**, 361 (1990).
[9] S. E. Ulloa, E. Castaño, and G. Kirczenow, Phys. Rev. B **41**, 12 350 (1990).
[10] R. Cusco (private communication).
[11] R. L. Schult, D. G. Ravenhall, and H. W. Wyld, Phys. Rev. B **39**, 5476 (1989).
[12] E. Castaño and G. Kirczenow, Solid State Commun. **70**, 801 (1989).
[13] D. W. L. Sprung, Hua Wu, and J. Martorell (unpublished).
[14] E. Kühn, Arch. Elek. Übertragung **27**, 511 (1973).